AFRL-RX-WP-TP-2011-4206

A WEAKEST-LINK APPROACH FOR FATIGUE LIMIT OF 30CrNiMo8 STEELS (PREPRINT)

S. Ekwaro-Osire and H.V. Kulkarni

Texas Tech University

MARCH 2011

AIR FORCE RESEARCH LABORATORY
MATERIALS AND MANUFACTURING DIRECTORATE
WRIGHT-PATTERSON AIR FORCE BASE, OH 45433-7750
AIR FORCE MATERIEL COMMAND
UNITED STATES AIR FORCE

REPORT DOCUMENTATION PAGE

Form Approved
OMB No. 0704-0188

1. REPORT DATE *(DD-MM-YY)*	2. REPORT TYPE	3. DATES COVERED *(From - To)*
March 2011	Journal Article Preprint	01 March 2011 – 01 March 2011

4. TITLE AND SUBTITLE
A WEAKEST-LINK APPROACH FOR FATIGUE LIMIT OF 30CrNiMo8 STEELS (PREPRINT)

5a. CONTRACT NUMBER
In-house

5b. GRANT NUMBER

5c. PROGRAM ELEMENT NUMBER
62102F

6. AUTHOR(S)
S. Ekwaro-Osire and H.V. Kulkarni

5d. PROJECT NUMBER
4347

5e. TASK NUMBER
20

5f. WORK UNIT NUMBER
LM121100

7. PERFORMING ORGANIZATION NAME(S) AND ADDRESS(ES)
Texas Tech University
Department of Mechanical Engineering
Lubbock, TX

8. PERFORMING ORGANIZATION REPORT NUMBER
AFRL-RX-WP-TP-2011-4206

9. SPONSORING/MONITORING AGENCY NAME(S) AND ADDRESS(ES)
Air Force Research Laboratory
Materials and Manufacturing Directorate
Wright-Patterson Air Force Base, OH 45433-7750
Air Force Materiel Command
United States Air Force

10. SPONSORING/MONITORING AGENCY ACRONYM(S)
AFRL/RXLM

11. SPONSORING/MONITORING AGENCY REPORT NUMBER(S)
AFRL-RX-WP-TP-2011-4206

12. DISTRIBUTION/AVAILABILITY STATEMENT
Approved for public release; distribution unlimited.

13. SUPPLEMENTARY NOTES
PAO Case Number: 88ABW 2010-3612; Clearance Date: 30 June 2010. Document contains color.
Journal article submitted to the *Journal of Engineering Materials and Technology*.

14. ABSTRACT
The transfer of fatigue data from laboratory specimens to field components under multiaxial fatigue is a difficult task. This is particularly the case in the transfer of data from specimens with well-defined shapes to components in the field with arbitrary shapes. A number of effects are to be considered in the transfer of data from a laboratory specimen to a field component. These effects include: pure size effect, pure gradient effect or notch size effect, and load type effect. The research question for this study was: Can an effective weakest-link approach for the fatigue limit of 30CrNiMo8 steels be developed? The specific aims constructed to address the research question were: (1) to develop an algorithm for the weakest-link approach to capture the pure size effect; (2) to perform verification studies on the algorithm for the weakest-link approach; and (3) to investigate volume effect and other effects on predictions of the probabilities of failure. The theory of the weakest-link formulation combined with the Dang Van fatigue failure criteria was used to develop an algorithm for the calculated probability of failure.

15. SUBJECT TERMS
fatigue, multiaxial fatigue, weakest-link, 30CrNiMo8

16. SECURITY CLASSIFICATION OF:			17. LIMITATION OF ABSTRACT:	18. NUMBER OF PAGES	19a. NAME OF RESPONSIBLE PERSON (Monitor)
a. REPORT	b. ABSTRACT	c. THIS PAGE			Andrew Rosenberger
Unclassified	Unclassified	Unclassified	SAR	34	19b. TELEPHONE NUMBER *(Include Area Code)* N/A

A Weakest-Link Approach for Fatigue Limit of 30CrNiMo8 Steels

S. Ekwaro-Osire[1] and H.V. Kulkarni

Department of Mechanical Engineering, Texas Tech University, Lubbock, USA

Abstract

The transfer of fatigue data from laboratory specimens to field components under multiaxial fatigue is a difficult task. This is particularly the case in the transfer of data from specimens with well-defined shapes to components in the field with arbitrary shapes. A number of effects are to be considered in the transfer of data from a laboratory specimen to a field component. These effects include: pure size effect, pure gradient effect or notch size effect, and load type effect. The research question for this study was: Can an effective weakest-link approach for the fatigue limit of 30CrNiMo8 steels be developed? The specific aims constructed to address the research question were: (1) to develop an algorithm for the weakest-link approach to capture the pure size effect; (2) to perform verification studies on the algorithm for the weakest-link approach; and (3) to investigate volume effect and other effects on predictions of the probabilities of failure. The theory of the weakest-link formulation combined with the Dang Van fatigue failure criteria was used to develop an algorithm for the calculated probability of failure. The verification results of the proposed algorithm were presented. For cylindrical specimens under tension-compression loading, the probability of failure with the use of the Dang Van failure criterion was compared to predictions generated by other failure criteria. The results of using the proposed formulation to predict the fatigue limit of 30CrNiMo8 steel cylindrical specimens were presented and discussed. The weakest-link approach developed was shown to predict the pure size effect of 30CrNiMo8 steel cylindrical specimens under tension-compression fatigue loading. The calculations of the probability of failure of cylindrical specimens were shown to be in good agreement with the published results.

[1] Corresponding author: Department of Mechanical Engineering, Texas Tech University, Lubbock, TX 79409, USA, stephen.ekwaro-osire@ttu.edu, 806.742.3563 Ext 232, 806.742.3540 (FAX).

1 Background

1.1 Effects on the Fatigue Limits of Steels

The transfer of fatigue data from laboratory specimens to field components under multiaxial fatigue is a difficult task. This is particularly the case in the transfer of data from specimens with well-defined shapes to components in the field with arbitrary shapes. A number of factors are to be considered in the transfer of data from a laboratory specimen to a field component. These factors that often influence the fatigue data include: pure size effect, pure gradient effect or notch size effect, and load type effect.

In the case of the four-point rotating bending configuration, if tests are performed on specimens of the same radius and of different lengths, the results can be used to investigate pure size effect [1, 2]. Alternatively, in the case of fully reversed tension-compression, if tests are performed on specimens of the same radius and of different lengths, the results can also be used to investigate the pure size effect.

Pure gradient effect is also referred to as the volumetric stress distribution effect by some authors [3]. Morel and Palin-Luc [3] assert that the pure gradient effect is more important than the pure size effect. The pure gradient effect can be either a normal stress gradient effect or a shear stress gradient effect. The notch size effect is a form of pure stress gradient effect, but because of the particularly high stress gradient, it involves high stress-strain concentrations that create a local plasticity effect [3]. Some authors refer to the notch size effect as the stress-strain gradient effect [4, 5]. It has been noted that use of tests with notched specimens to investigate the pure gradient effect may be problematic since a local plasticity effect is often in play [3].

The load type effect has also been referred to as the mechanical size effect by some authors. A load type effect is due to the type of mechanical loading [6]. The mechanical loading types include: tension-tension, tension-compression, rotating bending, cantilever bending, and torsion. Smooth cylindrical specimens of the same size, under tension and/or compression loading, rotating bending, and cantilever bending, exhibit different fatigue strengths while the local stress state is the same [5]. In this particular case, cantilever bending fatigue strength is highest, followed by the rotating bending fatigue strength, and then by the tension and/or compression fatigue strength [1, 6].

1.2 Experiments

Various experimental studies have been carried out to demonstrate the effects that impact the fatigue limits. Bomas and Schleicher [7] performed experimental studies on 16MnCrS5 cylindrical specimens with no notches and with V-notches. For the unnotched specimens, 6 mm gage diameters with various lengths were used. For the specimens with V-notches, 6 mm gage diameters with various notch tip radii were used. In these studies, the cyclic loads used were due to rotating bending, alternating torsion, tension-compression, and repeated tension. For the specimens with no notches, the surface carbon content, surface oxidation, and surface roughness also varied.

Bomas and co-workers [8, 9] performed experiments on bearing steel SAE 52100 specimens. A set of the specimens had no notches, while another set had V-notches of two geometries. The loads applied included rotating bending, alternating torsion, tension-compression, and repeated tension. They demonstrated a size and notch effect and analyzed the crack initiation at the surface and volume. Sonsino [10] considered size effect of cylindrical specimens with fillets exposed to fully reversible plane bending. Using a fully developed S-N curve, he showed the impact of the specimen size on the fatigue strength of the metal. Du Quesnay et al. [11] analyzed the notch-size effects at the fatigue limit of flat specimens with circular notches in the center. The materials used in the investigation were 2024-T351 aluminum alloy and SAE 1045 steel. A geometrical size effect of cylindrical specimens with V-notches and no notches was experimentally investigated by Larsson [12]. The materials used in the investigations were carbon steel SS 1650 and alloy steel SS 2541-03. A geometrical size effect was shown to exist even for the unnotched specimens under uniaxial tension for which the stress gradient below the material surface is zero. Hatanaka and co-workers [13] experimentally investigated the size effect on rotating bending fatigue of specimens made out of forged steel JIS SF 50 and cast steel JIS SCMn 2A. Cylindrical specimens with no notches of various gage diameters were used. It was shown that the fatigue limits (strength) decreased with an increase in the specimen size. Furthermore, it was also shown that the size effect for forged steel was about twice as large as that of cast steel.

Kloos et al. [14] considered the geometrical size effect in 37Cr4 steel specimens with and without V-notches. The specimens were exposed to rotating-bending loading or tension-compression loading. For the specimens without notches under rotating-bending loading, it was observed that the fatigue limit decreased as the specimen diameter increased. For the specimens with V-notches under tension-compression loading, it was observed

that the fatigue limit decreased asymptotically as the specimen diameter increased. For V-notched specimens tested in rotating bending, a strong dependence of the fatigue limit on the specimen diameter was observed.

In his dissertation, Magin [15] experimentally investigated the size effect of cylindrical specimens with no notches and with V-notches subjected to rotating bending. The material selected in this study was 30CrNiMo8. The number of cycles used to define fatigue limit were 10^7. The staircase method was used to evaluate the fatigue limits. Böhm [16, 17] used the same material when considering cylindrical specimens with no notches and with V-notches exposed to alternating tension-compression (R = -1). He used a total of 310 specimens for his study. Here the number of cycles at the endurance limit was chosen to be 2×10^6.

1.3 Weakest-Link Approaches

Weibull [18] introduced a statistical concept based on the "weakest-link" to account for statistical size effect. From this theory, it can be observed that the probability of failure increases with an increasing volume of the component. For components subjected to an alternating load, an increased probability of failure corresponds to a lower fatigue limit of larger components. It has been argued that, although initially formulated for brittle materials under static loading, the weakest-link theory can be transferred to metals under fatigue loading. In part this assertion can be justified by the observation that as with brittle materials, fatigue failure of metals is due to the presence of randomly distributed initial flaws or defects [2]. In contexts of fatigue, a hypothesis can be formulated as: A component subjected to an alternating load forms a sample of initial cracks at the end of the crack initiation phase. The larger the component, the larger the sample of the cracks will be [19]. A difficulty with the weakest-link principle is that neither the probability density distribution of the initial crack nor the number of cracks in a sample is readily available. The weakest-link theory consists of a power law without a characteristic size or length [20]. In their study, Morel and Flacelière [21] show that the weakest-link approach can be used in the finite and infinite fatigue life regimes, provided that a proper equivalent stress is introduced and a relevant damage model is applied.

The weakest-link approach is based on the view that flaws or defects are statistically distributed in the volume of a material. The approach is anchored on the following assumptions [2, 4]: the structure is considered as a chain that consists of a series links; the failure of the weakest link generates the fracture of the whole structure, and the size of flaws is very small compared to the distance between them (thus, there is no interaction between flaws).

By use of a power-law relationship between the critical flaw size and the applied stress and on the assumption that the maximum defect size follows a two-parameter Fréchet distribution, the probability of failure can be formulated [4, 22]. Generally, the weakest-link formulation is only applicable to problems of fatigue crack initiation since fatigue crack propagation is not described by the model [7]. Thus, when applying the weakest-link model to a given body, it is assumed that crack initiation induces failure in the body.

1.4 Applications of Weakest-Link Approaches

Makkonen [19] presented a statistical model for the statistical size effect, due to the sample size, in the fatigue limit of steels. In this method, the statistics of extremes was used to estimate the largest crack to be expected in the specimens with variation in surface area. The parent population of initiated cracks was assumed to follow a lognormal distribution. By use of linear elastic fracture mechanics, a connection between the largest initiated crack and the fatigue limit was established. This method is particularly effective if the relationship between the static strength and thickness, and the scatter and thickness is available. Using an augmented version of the weakest-link approach, Makkonen [23, 24] explained the connection between size effect and notch-size effect in steels. The results obtained from the model were compared to a series of experimental results from the literature. Lanning et al. [25] proposed a weakest-link notch model based on surface area stresses. The predictions of the model were compared to experimental results. Due to the localized plastic straining and negative stress ratios, the model showed some inaccuracies.

Flacelière and Morel [2] presented two weakest-link formulations: one that uses an integration over the surface and another that uses an integration over the volume. The models predicted fatigue data scatter for various loading conditions for mild steel and a nodular cast iron. Both models were able to account for the gradient effect and the size effect. The volume formulation was able to account for the decrease of the fatigue limit with the size of the specimen, as shown in experiments. An extended weakest-link formulation was used to predict the fatigue limit of notched and multiaxially loaded specimens of carburized steel [7]. The model was shown to be effective in calculation of the endurance limits and the local fracture probabilities of steel.

Delahay and Palin-Luc [4] combined the weakest-link concept with a deterministic energy-based high-cycle multiaxial fatigue criterion. The predictions by this probabilistic model were in very good agreement with experimental results for specimens without notches. Furthermore, the model was able to predict the size effect.

Doudard et al. [26] proposed a probabilistic framework to model multiaxial high cycle fatigue tests. The framework was based on a Poisson point distribution of the sites to describe the gradual activation of microplasticity. This model accounted for the stress heterogeneity, scatter of fatigue data, and size effects. The model was shown to be in good agreement with experimental results. Palin-Luc and Saintier [5] presented a volumetric energy-based approach that combines the weakest-link concept with a non-local model. The approach handles multiaxial fatigue crack initiation problems. The approach takes into account the notch-size effect and load type effect.

Wormsen et al. [22] presented a non-local stress approach for fatigue assessment based on weakest-link theory and the statistics of extremes. This method considered the whole stress field rather than just the highest local stress while performing the analysis. The starting point of the computation was the statistical distribution of fatigue strength data from the unnotched specimens. The predictions of the approach compared favorably with experimental results from the literature [16, 17]. It was further shown that the weakest-link concept is able to predict the different fatigue strengths observed for tension-compression loading, rotating bending, and alternating axial bending, respectively [6].

1.5 Research Question and Scope of Work

The research question in this paper was: Can an effective weakest-link approach for the fatigue limit of 30CrNiMo8 steels be developed? The specific aims developed to address the research question are: (1) to develop an algorithm for the weakest-link approach to capture the pure size effect; (2) to perform verification studies on the algorithm for the weakest-link approach; and (3) to investigate volume effect and other effects on predictions of the probabilities of failure.

The theory behind the weakest-link approach was presented. The volume model with two-parameter Weibull distribution was developed. Algorithms to calculate the probability of failure for fatigue analysis by the weakest-link approach was developed. Finite element analysis was performed in ANSYS to calculate the stresses generated in the specimens. The MATLAB program was developed to process the stresses and to calculate the probability of failure of specimens in static and fatigue. The results of probabilities of failure were compared with the results from the literature. The effects of volume of specimen, Weibull modulus, and formulation of effective stress amplitude on the probability of failure were investigated. The weakest-link formulation was used to predict

the pure size effect of 30CrNiMo8 steels obtained experimentally in the literature. The predictions were compared to the experimental results, and the errors were assessed.

2 Methodology

2.1 Theory and Algorithm

In the weakest-link theory, the probability of failure of a steel specimen due to volume flaws can be described by [27]:

$$P_f = 1 - \exp\int_v \left[-f(\sigma)\left(\frac{dV}{V_u}\right)\right], \tag{1}$$

for two-parameter distribution:

$$f(\sigma) = \left(\frac{\sigma_{eq}}{\sigma_o^*}\right)^m, \tag{2}$$

where P_f, is the probability of failure, σ_{eq}, is the equivalent stress amplitude, σ^*_o, is the scale parameter, V_u, is the unit volume, and m, is the Weibull modulus, also called as shape parameter, which is a measure of scatter in the fatigue strength of normally identical components. In this thesis, the two-parameter weakest-link theory is used, and σ^*_o, is referred to as the characteristic fatigue limit of the reference fatigue test specimen.

Substituting Eq. (2) in Eq. (1), the probability of failure of a steel specimen due to volume flaws for two-parameter weakest-link formulation can be given by [27, 28]:

$$P_f = 1 - \exp\int_v \left[-\left(\frac{\sigma_{eq}}{\sigma_o^*}\right)^m \right]\left(\frac{dV}{V_u}\right). \tag{3}$$

Eq. (3) is the CDF (cumulative distribution function) of the two-parameter weakest-link approach. Characteristic fatigue limit, σ^*_o, and Weibull modulus, m, are the experimental quantities.

The characteristic fatigue limit, σ^*_o, can be related to the fatigue strength per unit volume, σ_u, with the relationship:

$$\sigma_o^* = \frac{V_u^{1/m}\sigma_u}{\Gamma(1+1/m)}. \tag{4}$$

Substituting Eq.(4) into Eq.(3) yields a two-parameter weakest-link formulation for volume flaws [29]:

$$P_f = 1 - \exp\left[-\left(\frac{1}{m}!\right)^m \left(\frac{\sigma_{nom}}{\sigma_u}\right)^m \frac{V}{V_u} \sum(V) \right], \tag{5}$$

where $(1/m)! = \Gamma\left[1 + (1/m)\right]$ with Γ is the gamma function and σ_{nom} is the nominal stress. To calculate probability of failure using Eq.(5), the parameters m, σ_u, V_u, and σ_{nom}, are required. The nominal stress, σ_{nom}, is the maximum equivalent stress amplitude, which is purely a numerical quantity and has no influence on the probability of failure result in Eq. (5). The term $\sum(V)$ in Eq. (5) was expressed as [29]:

$$\sum(V) = \frac{1}{V} \int_v \frac{1}{4\pi} \int_{B_u} \left(\frac{\sigma_{eq}}{\sigma_{nom}}\right)^m dB_u dV. \tag{6}$$

In the numerical calculation of the term $\sum(V)$, the following formulation was used [29]:

$$\sum(V) = \sum_{i=1}^{N_s} \frac{V_i}{V} \Sigma(V_i), \tag{7}$$

where (V_i) is the volume of element i. N_s, is the number of effective elements, and $\sum(V_i)$, is the stress volume integral for element i, given by [29]:

$$\sum(V_i) = \frac{1}{V_i} \int_{v_i} F_i dV_i, \tag{8}$$

where F_i is given by [29]:

$$F_i = \frac{1}{4\pi} \int_{B_u} \left(\frac{\sigma_{eq}}{\sigma_{nom}}\right)^m dB_u. \tag{9}$$

The integration over B_u, in Eq. (9) is referred to as the orientation integration. After the orientation integration is performed, the term $\sum(V_i)$, is calculated by means of Eq. (8) by Gauss-Legendre integration. For the Gauss-Legendre integration, the stresses are sampled at N_g, Gauss points and then the weight factors w^i_k, are calculated for each of the Gauss points. The Gauss points are those points for which the Gauss-Legendre integration is performed. The F_i's are calculated for each Gauss point, k, and then combined with the respective weight factors w^i_k, to yield $\sum(V_i)$. After combination of F_i, and w^i_k, Eq. (8) can then be reformulated as [29]:

$$\sum(V_i) = \frac{1}{V_i} \sum_{k=1}^{N_g} F_k^i w_k^i. \tag{10}$$

The integration errors can lead to large errors in P_f, because, σ^m_{eq}, varies strongly for larger values of m. Hence, we can use a measure which is not so sensitive to integration errors given by the predicted mean value of σ_{nom}.

$$\overline{\sigma}_{nom} = \sigma_u \left[\frac{V_u}{V \sum (V)} \right]^{1/m}. \tag{11}$$

Substituting Eq. (11) in Eq. (5) we get

$$P_f = 1 - \exp\left[-\left(\frac{1}{m}! \right)^m \left(\frac{\sigma_{nom}}{\overline{\sigma}_{nom}} \right)^m \right], \tag{12}$$

which gives the probability of the failure as the output of the algorithm.

2.2 Verification

The developed algorithms were verified to be accurate for static and fatigue analysis. The verification work involved the comparison of results generated by the algorithm and the results presented by other authors. The rectangular beam with dimensions 10mm × 4mm × 1mm under pure bending was used for verification of the algorithm in static loading, and Bohm's cylindrical smooth specimen with diameter 16 mm under tension was used for verification of the algorithm in fatigue loading. Table 1 summarizes the results for static analysis of a rectangular beam to calculate the probability of failure. The exact results for the probability of failure were calculated. The percentage errors were calculated with respect to the exact results. The table shows the comparison of probability of failure between the exact results, results obtained from commercial software, and our results obtained by using the algorithm for the weakest-link approach. The results show that the probability of failure decreases with an increase in the Weibull modulus. The Weibull modulus is the measure of the fatigue limit scatter and indirectly the scatter of the defect distribution. The large value of Weibull modulus implies small scatter of defects. The errors in the results were calculated and compared to the exact solution and to the authors' results

2.3 Analyses

The principle of independent action (PIA) theory is generally used in static analysis. The formulation of PIA theory can be given by [30]:

$$\sigma_{eq}^m = \langle \sigma_1 \rangle^m + \langle \sigma_2 \rangle^m + \langle \sigma_3 \rangle^m, \tag{13}$$

where σ_1, σ_2, and σ_3, are the principal stress amplitudes which are the results obtained from the ANSYS. For PIA formulation, principal stress amplitudes are assumed to be zero if they are negative [30]. Smart et al. [30, 31] used PIA theory for static analysis.

The maximum principal stress theory suggests that the failure occurs when the maximum principal stress exceeds the uniaxial tensile yield strength. The maximum of the three principal stresses is used as equivalent stress. The formulation for maximum principal stress theory is given by [32]:

$$\sigma_1 \leq \sigma_y, \tag{14}$$

where σ_1 is the maximum principal stress and σ_y is the yield strength.

The weakest-link theory assumes that the defects determine the fatigue limit. Defects such as non-metallic inclusions and pores tend to grow in a direction perpendicular to the maximum principal stress range. Hence in some instances, the maximum principal stress theory has been used with the weakest-link theory [32].

In the last two decades, the Dang Van fatigue failure criterion has been widely used in industry. The model accounts for the orientation distribution of grains, employing a micro plasticity analysis to assess the intensity of local plastic strain within individual grains. Although the small fatigue crack growth behavior is not described by this approach, the elastic shakedown of cyclic micro plasticity response is considered as the another source of fatigue limit [27]. The Dang Van criterion can be expressed as follows [27, 33, 34]:

$$\tau_{\max}(t) + p\sigma_H(t) = \sigma_{eq}, \tag{15}$$

where the instantaneous hydrostatic component of the stress tensor is

$$\sigma_H(t) = \frac{\sigma_{11} + \sigma_{22} + \sigma_{33}}{3}, \tag{16}$$

and the instantaneous value of Tresca shear stress is

$$\tau_{\max}(t) = \frac{s_1(t) - s_2(t)}{2}. \tag{17}$$

This shear stress is evaluated over a symmetrized stress deviator, which is obtained by subtracting $\delta_{ij}\sigma_H(t)$, from the stress deviator:

$$s_{ij}(t) = \sigma_{ij}(t) - \delta_{ij}\sigma_H(t), \tag{18}$$

$$\hat{s}_{ij}(t) = s_{ij}(t) - s_{ij,m}. \tag{19}$$

The coefficient p, is dependent on the material properties and is given by [34-36]:

$$p = 3\left(\frac{t_{-1}}{f_{-1}}\right) - \sqrt{3}. \tag{20}$$

For hard metals with ultimate strength higher than 680 MPa, the ratio in Eq. (20) has to satisfy the relationship [35, 37]

$$0.577 \le \frac{t_{-1}}{f_{-1}} \le 0.8, \tag{21}$$

where t_{-1}, and f_{-1}, are, respectively, the fatigue limits under fully reversed torsion and fully reversed bending. The standard deviations of 5% for reversed tension and reversed bending fatigue limits were considered in the calculation of the coefficient p, for the Dang Van criterion.

Because of the symmetrization of the stress deviator, the term $\tau_{max}(t)$, alone is unable to account for the effect of normal stresses upon the fatigue limit; hence, the effect of a mean normal stress upon fatigue limits in bending and torsion is taken into account by term $p\sigma_H(t)$. This term represents the effect of the hydrostatic stress on crack nucleation.

The PIA theory was used for static analysis of the rectangular beam under pure bending. The fatigue analysis of a cylindrical specimen was performed by means of the maximum principal stress theory and the Dang Van criterion. The probability of failure against applied stress was plotted for different values of applied stresses. The two different formulations of stresses can be compared from the plot.

By the use of Eq. (4) in Eq. (5), the probability of failure of the specimen can be formulated as:

$$P_f = 1 - \exp\left[-\left(\frac{\sigma_{nom}}{\sigma_o^*} \right)^m V \sum(V) \right] \tag{22}$$

where

$$\sigma_o^* = \sigma_o \left(\frac{V}{V_u} \right)^{1/m}, \tag{23}$$

and where σ_o is the parameter which depends on the volume of the material (fatigue limit), and σ^*_o is independent of the volume and depends on the material property [38]. From Eq. (22) and Eq. (23) we get:

$$P_f = 1 - \exp\left[-\left(\frac{\sigma_{nom}}{\sigma_o} \right)^m \sum(V) \right]. \tag{24}$$

$$P_f = 1 - \exp\left[-\left(\frac{\sigma_{nom}}{\sigma_o} \right)^m \frac{1}{V} \int_v \frac{1}{4\pi} \int_{B_u} \left(\frac{\sigma_{eq}}{\sigma_{nom}} \right)^m dB_u dV \right]. \tag{25}$$

$$Pf = 1 - \exp\left[-\left(\frac{\sigma'_{eq}}{\sigma_o} \right)^m \right], \tag{26}$$

$$Pf = 1 - \exp\left[-\left(\frac{\sigma'_{eq}}{\sigma^*_o} \right)^m \frac{V}{V_u} \right]. \tag{27}$$

where σ'_{eq} is the fatigue strength which is equivalent to all the equivalent stresses in the elements. The logarithmic form of Eq. (26) is given by:

$$\ln\ln\left(\frac{1}{1-Pf} \right) = m \ln \sigma'_{eq} - m \ln \sigma_o. \tag{28}$$

The plot of lnln(1-P_f) versus ln(σ'_{eq}) will provide the Weibull modulus m as the slope of the straight line. By use of Eq. (28) at lnln,(1-P_f) = 0 (when P_f = 0.632), $\sigma'_{eq} = \sigma_o$.

Consider two specimens of the same material with different volumes V_1, and V_2 and fatigue strengths σ'_{eq1}, and σ'_{eq2} subjected to same type of loading and constant value of probability of failure.

$$1 - \exp\left[-\left(\frac{\sigma'_{eq1}}{\sigma^*_0} \right)^m \frac{V_1}{V_u} \right] = 1 - \exp\left[-\left(\frac{\sigma'_{eq2}}{\sigma^*_0} \right)^m \frac{V_2}{V_u} \right]. \tag{29}$$

At lnln(1-P_f) = 0 (when P_f = 0.632), $\sigma'_{eq} = \sigma_o$. Hence we can write:

$$\sigma_{o1}{}^m V_1 = \sigma_{o2}{}^m V_2. \tag{30}$$

Hence, for a constant value of probability of failure (P_f = 0.632), the relation between fatigue limits of two components σ_{o1}, and σ_{o2}, with volumes V_1, and V_2, can be given by:

$$\frac{\sigma_{o1}}{\sigma_{o2}} = \left(\frac{V_2}{V_1} \right)^{1/m}. \tag{31}$$

The fatigue limit predictions were performed on Bohm's and Magin's [39, 40] smooth specimens of different volumes. The fatigue limits of two specimens were predicted from the fatigue limit of the first assumed standard specimen [32]. The fatigue limits of the specimens were plotted against the diameters of the specimens.

3 Results and Discussions

3.1 Theory and Algorithm

Fig. 1 shows the algorithm that was generated to calculate the probability of failure of the 30CrNiMo8 specimens by means of the weakest-link formulation. The input parameters for fatigue analysis were the Weibull modulus, m, the characteristic fatigue limit, σ^*_o, the fatigue limit in reversed torsion, t_{-1}, the fatigue limit in reversed bending, f_{-1}, and the specimen dimensions. The Weibull modulus and material parameters are extracted from experiments in the literature [27, 41]. The finite element modeling of specimen was performed using ANSYS. The stresses in the elements were generated using ANSYS for given specimen dimensions, applied stress, and material properties. The MATLAB program was developed to convert the stresses generated by ANSYS into equivalent stresses and calculate the probability of failure of the specimen. The MATLAB program consists of two subprograms. The first program calculates equivalent stresses from the stresses generated by ANSYS. The second program reads all the input parameters and equivalent stresses, and calculates the probability of failure. The program to calculate probability of failure uses a subroutine to calculate Gauss weight factors. As shown by the algorithm in Fig. 1, the stress amplitudes are imported into the MATLAB algorithm to calculate the effective stress amplitude. For fatigue analysis, the Dang Van criterion was used as the failure theory to calculate the equivalent stresses. The nominal stress σ_{nom} was selected as the value of maximum equivalent stress. It is used to obtain sensible values during numerical evaluation of theory and has no effect on the predicted value of probability of failure. Following this, the parameter, F_i, was calculated by Eq. (9). A standard MATLAB subroutine was used to calculate the weight factors, w_i^k. Then, the term $\sum(V_i)$ was evaluated by the Gauss-Legendre integration by means of Eq. (10). The term $\sum(V)$ was calculated by summation of $\sum(V_i)$, values, in a loop in Eq. (7). The term $\bar{\sigma}_{nom}$, which is the predicted mean value for σ_{nom}, was calculated by Eq. (11). After obtaining the $\bar{\sigma}_{nom}$ value, the algorithm then calculated the probability of failure of the specimen by means of Eq. (12) [29, 31]. The algorithm was developed enable efficient calculation of the probability of failure.

3.2 Verification

As an initial verification of the algorithm, it was modified for static analysis by change of the input and the failure criterion used to calculate the equivalent stress. The input parameters for static analysis used were Weibull modulus, m, unit mean strength σ_u, and, specimen dimensions. The PIA failure criterion was used in the calculation

of the equivalent stresses. Table 1 summarizes the results for static analysis of a rectangular beam to calculate the probability of failure. The exact results for the probability of failure were calculated. The percentage errors were calculated with respect to the exact results. The table shows the comparison of probability of failure between the exact results, results from commercial software (as cited in [42]),and our results obtained by use of the algorithm developed in this paper. The results show that the probability of failure decreases with an increase in the Weibull modulus. The Weibull modulus is the measure of the fatigue limit scatter and indirectly the scatter of the defect distribution. The large value of Weibull modulus implies small scatter of defects. The errors in the results compared to the exact solution and authors' results were calculated. The comparison showed that our results were close to the exact solution as compared to the results obtained by means of a commercial software [42]. For this verification study, an Intel Core 2 Duo 1.6 GHz processor required about 40 seconds to calculate the equivalent stresses using the ANSYS-generated stresses, and 10 seconds to calculate the probability of failure using the equivalent stresses.

After verification of the results by means of a static formulation, the algorithm was recast as a fatigue formulation as discussed in section 3.1 (see Fig. 1). Fig. 2 shows the plot of probability of failure, P_f, versus normalized effective stress amplitude, σ^*_{eq}, and applied stress, S. The probability of failure increases from 0 to 1 with an increase in normalized effective stress amplitude and applied stress. The trend of the plot is consistent with the results of Wormsen et al. [32] using similar parameters. Due to the increase in the load applied, there is an increase in equivalent stresses generated in the elements, and hence the probability of failure of specimen increases. The probability of failure increases instantaneously, as normalized effective stress amplitude increases above the characteristic fatigue limit. It should also be noted that when the normalized effective stress amplitude is unity, the probability of failure is 0.63. This indicates that the characteristic fatigue limit is the stress amplitude for which the probability of failure is 0.63 for the specified volume [29, 30, 32].

3.3 Analyses

Fig. 3 shows the plot of probability of failure, P_f, against applied stress, S, for PIA theory stress, the Maximum Principal Stress and the Dang Van criterion stress models [43]. The probability of failure increases from 0 to 1 with an increase in applied stress. For the Weibull modulus used in this case, the probabilities of failure calculated by Eq. (14) and Eq. (15) show minor differences. At higher values for the Weibull modulus, the two solutions will diverge. The PIA stresses and maximum principal stresses are very close because of very small values

for the second and third principal stresses and that in the PIA theory stress all negative stresses are set to zero. The maximum principal stresses and Dang Van criterion stresses show minor differences due to the difference in their formulation. The maximum principal stress theory determines the maximum value of the principal stress as the equivalent stress. The maximum principal stress theory can be used with the weakest-link theory due to the fact that defects such as non-metallic inclusions and pores tend to grow in a direction perpendicular to the maximum principal stress range. The Dang Van criterion uses the coefficient p, (Eq.(15)), which depends on the fatigue properties of the materials. The Dang Van criterion calculates the equivalent stress using the stresses generated in ANSYS as well as the material fatigue properties. The maximum principal stress theory and the Dang Van criterion are widely used in fatigue analysis.

Fig. 4 shows the plot of probability of failure, P_f, against applied stress, S, for 3 different specimens SB1, SB2, and, SB3 according to the Dang Van stress criterion. The probability of failure, P_f, increases with volume, V. The trend of the plot is consistent with the results from Kittl and Diaz [44, 45]. As the volume of the specimen increases, the number of defects increases, and hence there is an increase in probability of failure. The fatigue limit of the specimen decreases with an increase in size. For a constant applied stress and Weibull modulus, the probability of failure increases with an increase in volume.

Fig. 5 shows the plot of probability of failure, P_f, with respect to an increasing Weibull modulus, m. The probability of failure decreases in a monotonic manner with an increasing Weibull modulus. This behavior is consistent with that observed in the literature, in studies of problems involving the application of weakest-link theory to brittle materials under static loading [27].

The fatigue limit of specimens can be predicted by use of the size effect equation derived from the formulation in the algorithm. Fig. 6 shows the plots of fatigue limits against the diameters of the specimens. Here the first smaller diameter is used to predict the second and third larger diameters. The experimental and predicted fatigue limits are plotted. The experimental results used are a set selected from the data provided by Bohm's [39] smooth specimens.

Table 2 shows the experimental and predicted fatigue limits for Bohm's cylindrical smooth specimens. The percentage errors between experimental and predicted values are calculated. In this table, (i) in the third column, the 16 mm diameter is used to predict the values 38 mm and 76 mm diameter (also see Fig. 6); (ii) in the fifth column, the 38 mm diameter is used to predict the values 16 mm and 76 mm diameter; and (iii) in the seventh column, the

76 mm diameter is used to predict the values 16 mm and 38 mm diameter. The total average percentage error is 5.72 % which shows a degree of accuracy of prediction of size effect. Table 3 compares the predicted fatigue limits to experimental data from Magin [40] (this data was also used by other authors [22, 46] to verify theoretical results) and Hatanaka et al. [13] (this data was also used by other authors [47] to verify theoretical results). The results show that the algorithm presented in this paper is able to capture the size effect for cylindrical smooth specimens under tension-compression fatigue loading and specimens under rotating-bending fatigue loading. While still within an acceptable range, the predicted results are slightly better for specimens under tension-compression than those under rotating-bending fatigue loading.

4 Conclusion

The research question for this study was: Can an effective weakest-link approach for the fatigue limit of 30CrNiMo8 steels be developed? The specific aims constructed to address the research question were: (1) to develop an algorithm for the weakest-link approach to capture the pure size effect; (2) to perform verification studies on the algorithm for the weakest-link approach; and, (3) to investigate volume effect and other effects on predictions of the probabilities of failure.

The theoretical basis of the weakest-link approach for fatigue limit of 30CrNiMo8 steels was presented. An efficient algorithm to calculate the probability of failure using ANSYS and MATLAB was developed. The developed algorithm was initially verified by recasting the fatigue algorithm in a static formulation. The result obtained using this formulation was in good agreement with the exact solutions published in the literature. The next verification was performed using the fatigue formulation to calculate the probability of failure for a range of loading. The results obtained were consistent with those published in the literature.

The effects of formulation of equivalent stress theory, change in specimen volume, and Weibull modulus on the probability of failure were investigated. Due to the type of loading and the specimen geometry, there was no major difference between formulation of equivalent stress amplitudes by use of the maximum principal stress theory and by use of the Dang Van theory. The probability of failure increased with an increase in the volume of specimens due to an increase in the number of defects. The probability of failure decreased monotonously with increase in the Weibull modulus, which was consistent with published results. The weakest-link formulation was used to predict the pure size effect of 30CrNiMo8 steels obtained experimentally in the literature. The predictions were in good

agreement with the experimental results. In future work, the weakest-link approach presented in this paper for the fatigue limit of 30CrNiMo8 steels will be extended to predict the notch-size effect for cylindrical notched specimens.

5 Nomenclature

m = Weibull modulus

P_f = Probability of failure

σ_{eq} = Equivalent stress amplitude, MPa

σ_0^* = Characteristic fatigue limit, MPa

σ_0 = Fatigue limit, MPa

σ_u = Strength per unit volume

σ_{nom} = Nominal stress, MPa

$\bar{\sigma}_{nom}$ = Mean predicted value of nominal stress, MPa

σ_{eq}' = Fatigue strength MPa

V_u = Unit volume

S = Applied stress, MPa

σ^*_{eq} = Normalized effective stress amplitude

w_i^k = Gauss weight factor

N = Number of elements

N_g = Number of Gauss points

d = Diameter of the specimen, mm

τ = Shear Stress, MPa

σ_{H} = Hydrostatic Stress, MPa

p = Coefficient in Dang Van criterion

t_{-1} = Fatigue limit in reversed torsion MPa

f_{-1} = Fatigue limit in reversed bending MPa

6 Acknowledgments

The first author acknowledges the support of the Air Force Summer Faculty Fellowship Program during his 2008 summer tenure at the AFRL, Dayton, Ohio. Furthermore, the first author acknowledges the technical discussions with Dr. R. John and Dr. J.M. Larsen on this topic during his tenure at the AFRL.

7 References

[1] Papadopoulos, I. V., and Panoskaltsis, V. P., 1996, "Invariant Formulation of a Gradient Dependent Multiaxial High-Cycle Fatigue Criterion," Engineering Fracture Mechanics, 55, pp. 513-528.

[2] Flacelière, L., and Morel, F., 2004, "Probabilistic Approach in High-Cycle Multiaxial Fatigue: Volume and Surface Effects," Fatigue and Fracture of Engineering Materials and Structures, 27, pp. 1123-1135.

[3] Morel, F., and Palin-Luc, T., 2002, "A Non-Local Theory Applied to High Cycle Multiaxial Fatigue," Fatigue and Fracture of Engineering Materials and Structures, 25, pp. 649-665.

[4] Delahay, T., and Palin-Luc, T., 2006, "Estimation of the Fatigue Strength Distribution in High-Cycle Multiaxial Fatigue Taking into Account the Stress-Strain Gradient Effect," International Journal of Fatigue, 28, pp. 474-484.

[5] Palin-Luc, T., and Saintier, N., 2007, "Simulation of the Stress-Strain Gradient Effect to Design Safe Components against Multiaxial Fatigue," Materialprüfung, 49, pp. 370-377.

[6] Gaenser, H.-P., 2008, "Some Notes on Gradient, Volumetric and Weakest Link Concepts in Fatigue," Computational Materials Science, 44, pp. 230-239.

[7] Bomas, H., and Schleicher, M., 2005, "Application of the Weakest-Link Concept to the Endurance Limit of Notched and Multiaxially Loaded Specimens of Carburized Steel 16mncrs5," Fatigue and Fracture of Engineering Materials and Structures, 28, pp. 983-995.

[8] Bomas, H., Linkewitz, T., and Mayr, P., 1999, "Application of a Weakest-Link Concept to the Fatigue Limit of the Bearing Steel Sae 52100 in a Bainitic Condition," Fatigue and Fracture of Engineering Materials and Structures, 22, pp. 733-741.

[9] Bomas, H., Linkewitz, T., Mayr, P., Jablonski, F., Kienzler, R., Kutschan, K., Bacher-Höchst, M., Mühleder, F., Seitter, M., and Wicke, D., 1998, "Fehlstellenmodell Für Die Wechselfestigkeit," Materialprüfung, 40, pp. 58-63.

[10] Sonsino, C. M., 1993, "Zur Bewertung Des Schwingfestigkeitsverhaltens Von Bauteilen Mit Hilfe Örtlicher Beanspruchungen," Konstruktion, 45, pp. 25-33.

[11] Du Quesnay, D. L., Yu, M. T., and Topper, T. H., 1988, "An Analysis of Notch-Size Effects at the Fatigue Limit," Journal of testing and evaluation, 16, pp. 375-385.

[12] Larsson, B., 1985, "Geometrical Size Effect in Fatigue," eds., pp. 35-51.

[13] Hatanaka, K., Shimizu, S., and Nagae, A., 1983, "Size Effect on Rotating Bending Fatigue in Steels," Bulletin of the JSME, 26, pp. 1288-1295.

[14] Kloos, K. H., Buch, A., and Zankov, D., 1981, "Pure Geometrical Size Effect in Fatigue Tests with Constant Stress Amplitude and in Programme Tests," Zeitschrift für Werkstofftechnik, 12, pp. 40-50.

[15] Magin, W., 1981, "Untersuchung Des Geometrischen Grösseneinflusses Bei Umlaufbiegebeanspruchung Unter Besonderer Berücksictigung Technologischer Einflüsse," Ph.D. thesis, Technische Hochschule Darmstadt, Darmstadt, Germany.

[16] Böhm, J., 1980, "Zur Vorhersage Von Dauerschwingfestigkeiten Ungekerbter Und Gekerbter Bauteile under Berücksichtigung Des Statististischen Grösseneinflüsses," Ph.D. thesis, Technische Universität München, Munich, Germany.

[17] Böhm, J., and Heckel, K., 1982, "Die Vorhersage Der Dauerschwingfestigkeit Unter Berücksichtigung Des Statistishchen Grösseneinflusses," Zeitschrift für Werkstofftechnik, 13, pp. 120-128.

[18] Weibull, W., 1939, "A Statistical Theory for the Strength of Materials," Technical Report No. Swedish Royal Institute for Engineering Research, Stockholm.

[19] Makkonen, M., 2001, "Statistical Size Effect in the Fatigue Limit of Steel " International Journal of Fatigue, 23, pp. 395-402.

[20] Bazant, Z. P., 1999, "Size Effect on Structural Strength: A Review," Archive of Applied Mechanics, 69, pp. 703-725.

[21] Morel, F., and Flacelière, L., 2005, "Data Scatter in Multiaxial Fatigue: From the Infinite to the Finite Fatigue Life Regime," International Journal of Fatigue, 27, pp. 1089-1101.

[22] Wormsen, A., Sjodin, B., Härkegård, G., and Fjeldstad, A., 2007, "Non-Local Stress Approach for Fatigue Assessment Based on Weakest-Link Theory and Statistics of Extremes," Fatigue and Fracture of Engineering Materials and Structures, 30, pp. 1214-1227.

[23] Makkonen, M., 2003, "Notch Size Effect in the Fatigue Limit of Steel " International Journal of Fatigue, 25, pp. 17-26.

[24] Makkonen, M., 2003, "Response to Comments by Prof. Taylor On "Notch Size Effect in the Fatigue Limit of Steel" By M. Makkonen " International Journal of Fatigue, 25, pp. 781-783.

[25] Lanning, D. B., Nicholas, T., and Palazotto, A., 2003, "Hcf Notch Predictions Based on Weakest-Link Failure Models," International Journal of Fatigue, 25, pp. 835-841.

[26] Doudard, C., Hild, F., and Calloch, S., 2007, "A Probabilistic Model for Multiaxial High Cycle Fatigue," Fatigue and Fracture of Engineering Materials and Structures, 30, pp. 107-114.

[27] Flaceliere, L., and Morel, F., 2004, "Probabilistic Approach in High-Cycle Multiaxial Fatigue: Volume and Surface Effects," Fatigue & Fracture of Engineering Materials & Structures, 27, pp. 1123-1135.

[28] Fok, S. L., Mitchell, B. C., Smart, J., and Marsden, B. J., 2001, "A Numerical Study on the Application of the Weibull Theory to Brittle Materials," Engineering Fracture Mechanics, 68, pp. 1171-1179.

[29] Dortmans, L., Thiemeier, T., Brückner-Foit, A., and Smart, J., 1993, "Welfep: A Round Robin for Weakest-Link Finite Element Postprocessors," Journal of European Ceramic Society 11, pp. 17-22.

[30] Smart, J., Fok, S. L., 1994, "Discriminating between Volume and Surface Integral Theories for Brittle Materials," Engineering Fracture Mechanics, 48, pp. 801-810.

[31] Smart, J., Dortmans , L., Thiemeier, T., and Bruckner-Foit, A., 1992, "Welfep: A Round Robin for Weakest-Link Finite Element Postprocessors," Journal of the European Ceramic Society, pp. 17-22.

[32] Wormsen, A., Sjodin, B., Harkegard, G., Fjeldstad, A., 2007, "Non-Local Stress Approach for Fatigue Assessment Based on Weakest-Link Theory and Statistics of Extremes," Fatigue & Fracture of Engineering Materials & Structures, 30, pp. 1214-1227.

[33] Desimone, H., Bernasconi, A.,Beretta, S., 2005 "On the Application of Dang Van Criterion to Rolling Contact Fatigue " Politecnico di Milano,Dipartimento di Meccanica,

[34] Goncalves, C. A., and A., J., 2005, "Multiaxial Fatigue: A Stress Based Criterion for Hard Metals," International Journal of Fatigue, 27, pp. 177-187.

[35] Papadopoulos, I. V., and Panoskaltsis, V.P., 1996, "Invariant Formulation of a Gradient Dependent Multiaxial High-Cycle Fatigue Criterion," Engineering Fracture Mechanics, 55, pp. 513-528.

[36] Papadopoulos, I. V., Davoli, P.,Gorla, Filippini M. ,Bernasconi A. , 1997, "A Comparative Study of Multiaxial High-Cycle Fatigue Criteria for Metals " International Journal of Fatigue, 19, pp. 219-235.

[37] Sghaier, R., Bouraoui, Ch., Fathallah, R., Hassine T., Dogui A. , 2007, "Probabilistic High Cycle Fatigue Behaviour Prediction Based on Global Approach Criteria " International Journal of Fatigue, 29, pp. 209-221.

[38] Fett, T., Munz, D. , 1999, *Ceramics Mechanical Properties,Failure Behaviour,Material Selection*, Springer,

[39] Bohm, J., 1980, "Zur Vorhersage Von Dauerschwingfestigkeiten Ungekerbter Und Gekerbter Bauteile under Berücksichtigung Des Statististischen Grösseneinflüsses," Doctoral, Technische Universität München,

[40] Magin, W., 1981, "Untersuchung Des Geometrischen Grösseneinflusses Bei Umlaufbiegebeanspruchung Unter Besonderer Berücksictigung Technologischer Einflüsse," Doctoral, Technische Hochschule Darmstadt,

[41] Wormsen , A., Harkegard, G. , 2004, "A Statistical Investigation of Fatigue Behaviour According to Weibull's Weakest-Link Theory " 15th European Conference on Fracture,Stolkholm,Sweden,

[42] Powers, L. M., Nemeth N.N., 1991, "A Round Robin for Weakest-Link Finite Element Postprocessors (Welfep)," unpublished document,

[43] Mrzyglod, M., Zielinski, A. P., 2007, "Multiaxial High-Cycle Fatigue Constraints in Structural Optimization " International Journal of Fatigue, 29, pp. 1920-1926.

[44] Kittl, P., Diaz , G., 1988, "Weibull's Fracture Statistics, or Probabilistic Strength of Materials: State of the Art," Res Mechanica 24, pp. 99-207.

[45] Kittl, P., Diaz, G. , 1990, "Size Effect on Fracture Strength in the Probabilistic Strength of Materials " Reliability Engineering and System Safety 28, pp. 9-21.

[46] Makkonen, M., 1999, "Size Effect and Notch Size Effect in Metal Fatigue," Ph.D. thesis, Lappeenranta University of Technology, Lappeenranta, Finland.

[47] Carpinteri, A., Spagnoli, A., and Vantadori, S., 2002, "An Approach to Size Effect in Fatigue of Metals Using Fractal Theories," Fatigue and Fracture of Engineering Materials and Structures, 25, pp. 619-627.

[48] Powers, L. M., and Nemeth, N. N., 1991, "A Round Robin for Weakest-Link Finite Element Postprocessors (Welfep)," NASA unpublished document,

List of Figures

List of Tables

Figures

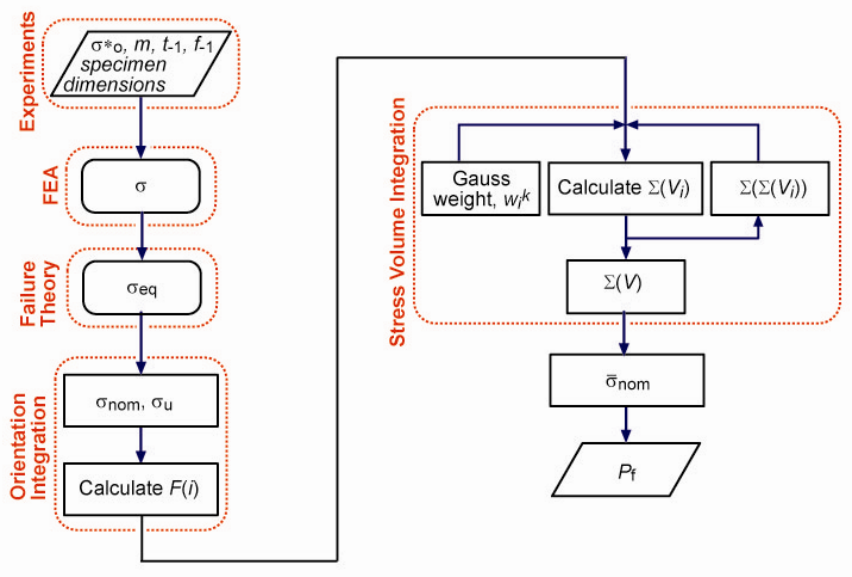

Fig. 1 Algorithm for weakest link approach for fatigue analysis

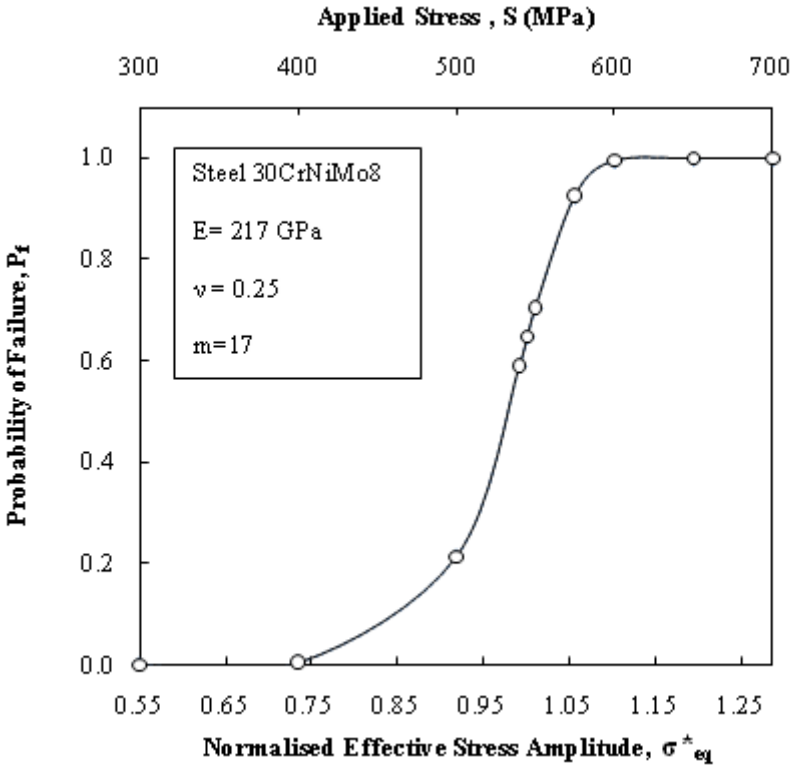

Fig. 2 Probability of failure as a function of normalized effective stress amplitude and applied stress

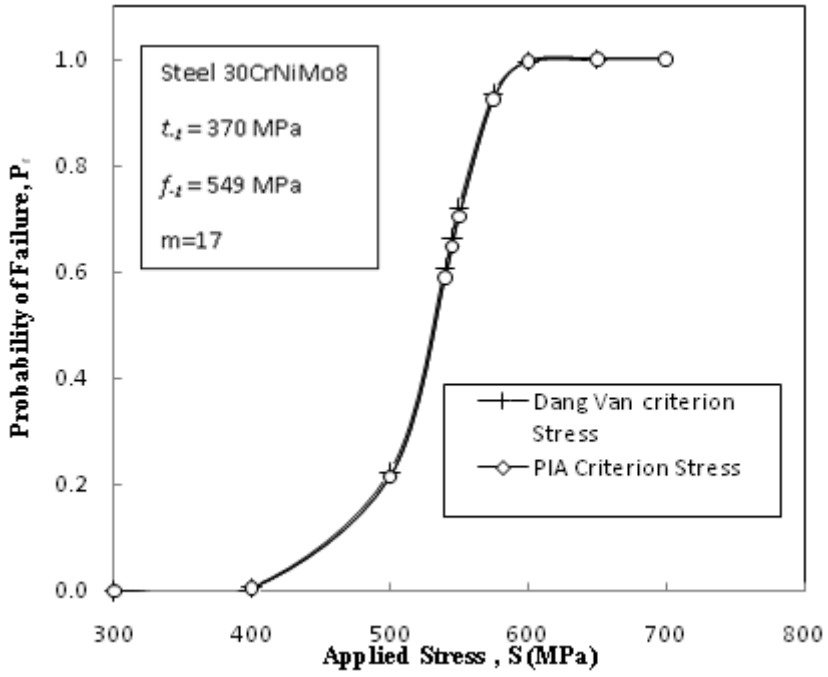

Fig. 3 Impact of the formulation of the equivalent stress on the probability of failure

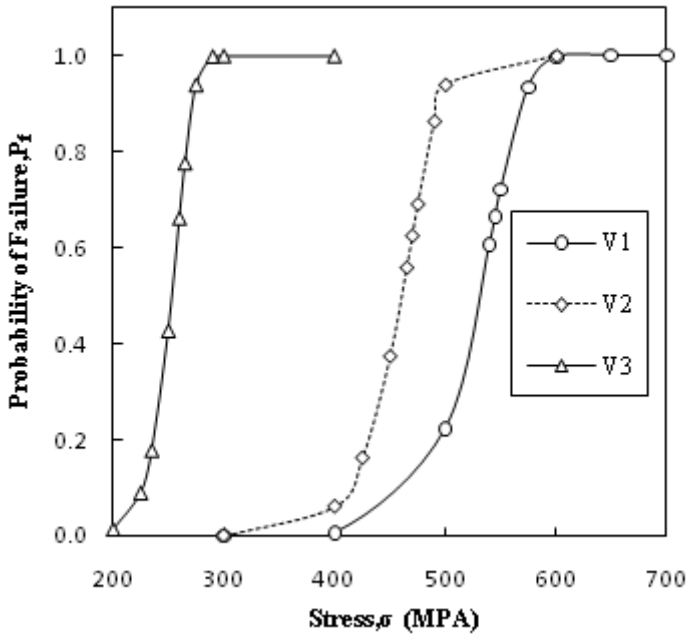

Fig. 4 Effect of volume on the probability of failure (V_1 = 1,193 mm^3, V_2 = 30,159 mm^3, V_3 = 201,873 mm^3)

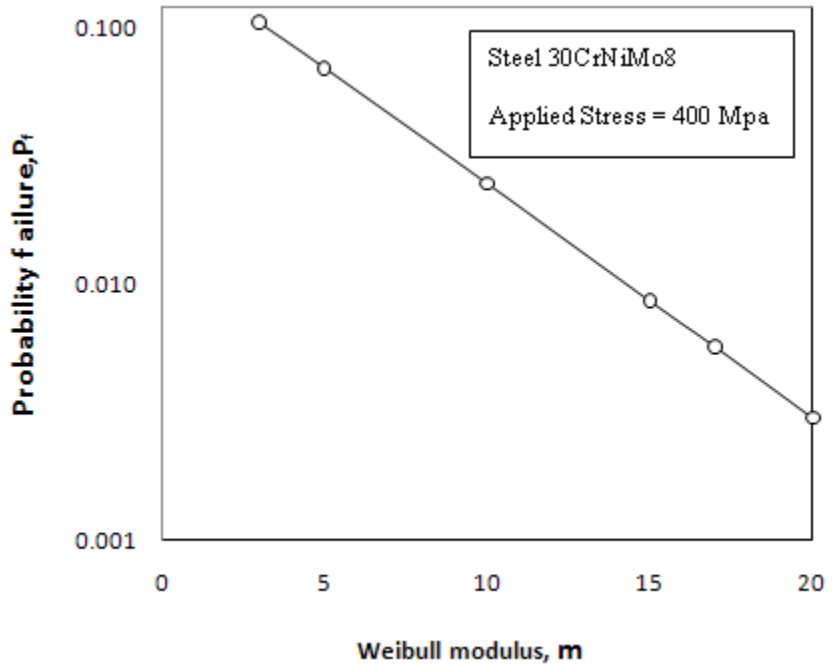

Fig. 5 Probability of failure as a function of Weibull modulus

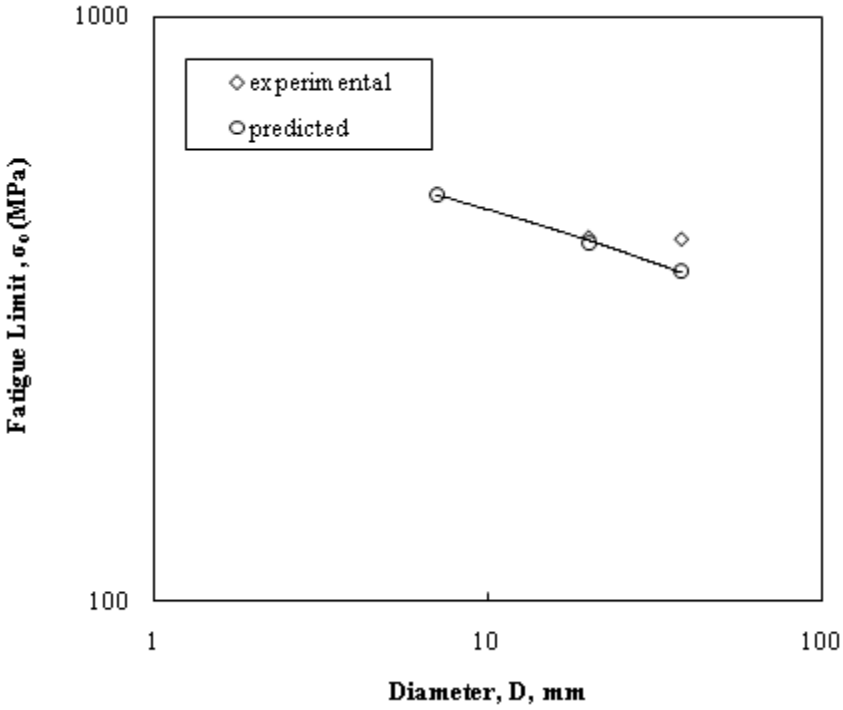

Fig. 6 Prediction of experimental fatigue limit by Böhm [16]

Tables

Table 1 Comparison of results with exact results for rectangular beam under pure bending

Weibull modulus	m	5	15	25
Scale Parameter	σ_{ov}	381.19	362.44	357.71
Mean Strength	σ_u	350.00	350.00	350.00
Nominal Strength	σ_{nom}	300.00	300.00	300.00
Exact Results [48]	$\bar{\sigma}_{nom}$	240.00	329.20	344.00
	P_f	0.87	0.14	0.02
Commercial Software Results [48]	$\bar{\sigma}_{nom}$	256.10	382.20	414.00
	P_f	0.76	0.02	0.00
Commercial Software Results [48]	$\bar{\sigma}_{nom}$	6.71	16.10	20.35
% error	P_f	11.96	88.60	99.01
Our Results	$\bar{\sigma}_{nom}$	233.08	350.20	349.43
	P_f	0.90	0.06	0.01
Our results	$\bar{\sigma}_{nom}$	2.88	6.38	1.58
% error	P_f	3.91	58.58	32.19

Table 2 Prediction of experimental fatigue limit by Böhm [16] (30CrNiMo8 Steel)

Diameter (mm)	σ_0 Experimental (MPa)	Predicted σ_0 using 16 mm specimen (MPa)	% error	Predicted σ_0 using 38 mm specimen (MPa)	% error	Predicted σ_0 using 76 mm specimen (MPa)	% error
16	496.00	496.00	0.00	507.88	2.40	563.92	13.69
38	420.00	410.17	2.34	420.00	0.00	466.34	11.03
76	417.00	366.77	12.04	375.56	9.94	417.00	0.00
		Average	4.79		4.11		8.24
Average percentage error = (4.79 + 4.11 + 8.24) / 3 = 5.72							

Table 3 Errors between predicted and experimental fatigue limits of cylindrical smooth steel specimens

Source	Steel	Cyclic Load	Number of Diameters	Average % error
Böhm [16]	30CrNiMo8	Tension-compression	3	5.72
Magin [15]	30CrNiMo8	Rotating-bending	5	7.68
Hatanaka et al. [13]	SCMn 2A	Rotating-bending	4	7.49
Hatanaka et al. [13]	SF 50	Rotating-bending	4	9.24